Kinetic Pathway of Gyroid-to-Cylinder Transition in Diblock Copolymer Melt under an Electric Field

Dung Q. Ly,[†] Takashi Honda,[‡] Toshihiro Kawakatsu,[§] and Andrei V. Zvelindovsky*,[†]

Centre for Materials Science, Department of Physics, Astronomy and Mathematics, University of Central Lancashire, PR1 2HE, United Kingdom; Japan Chemical Innovation Institute, and Department of Organic and Polymeric Materials, Tokyo Institute of Technology, Ookayama, Meguro-ku, Tokyo 152-8552, Japan; and Department of Physics, Tohoku University, Aoba Aramaki, Aoba-ku, Sendai 980-8578, Japan

Received August 15, 2006; Revised Manuscript Received February 13, 2007

ABSTRACT: Gyroid-to-cylinder transition in a diblock copolymer melt under an electric field is studied by real-space dynamical self-consistent-field theory. Starting from an equilibrium gyroid structure, we apply an electric field along [111], [1$\bar{1}$0], and [11$\bar{2}$] directions of the conventional unit cell of the gyroid structure. Under sufficiently high value of the electric field, an epitaxial transition to cylinders occurs. Contrary to the case of a similar transition under the shear flow, we observe 5-fold connections as intermediates in the transition. We found a critical behavior of the lifetime of the initial gyroid structure, which can be accounted for using the mean-field argument. Numerically obtained scattering function explains the unclarified intermediates experimentally observed in the thermal relaxation of a sheared gyroid.

1. Introduction

Diblock copolymers are composed of chemically different homopolymers covalently connected to one macromolecule. They can microphase-separate into various nanostructures. These nanostructures can be lamellar, cylindrical, gyroid, and spherical ones, which depends on the volume fraction of individual blocks and χN, where χ is the Flory−Huggins segmental interaction parameter that is inversely proportional to the temperature and N is the degree of polymerization.[1,2] Transition between different structures can be induced either by changing the temperature or by applying external fields. Among those are shear flow[2−9] and electric field.[10−16] For instance, Xu et al.[15] investigated experimentally and theoretically the sphere-to-cylinder transition in a diblock copolymer under an applied electric field. When a sufficiently strong electric field is applied, the spherical morphology transforms into hexagonally arranged cylinders. Transition to cylindrical morphology was also found under the influence of an applied shear flow.[3]

There are many open questions as to the existence and the stability of the so-called intermediate phases between the classical phases like lamellae and cylinders. Among these intermediate phases are the perforated lamellar phase (or mesh phase), the gyroid phase, etc.[17] Why are their regions in the phase diagram so different between the block copolymer and the short surfactant systems? How can these structures be stabilized?[17] Gyroid morphology is of great interest due to its bicontinuous nature of two mutually interpenetrating labyrinth networks, which can have many potential applications in chemical engineering such as catalytic membranes, photonic crystals, and so on.[18,19] These interpenetrating networks will lead to nontrivial rheological properties due to very complex possible topological transformations under external fields. However, the fundamental understanding of the gyroid structure is still limited compared to the classical phases like lamellae, cylinders, and spheres. To answer the questions associated with the stability of the intermediate phases, one needs to have a detailed knowledge on how, for instance, gyroid structure would respond to different types of external influences, like temperature change and various possible external fields. Matsen has studied the transition from gyroid to cylinders under temperature change with self-consistent-field calculation.[20] Recently, shear instability of the gyroid phase of a diblock copolymer was studied by the small-angle neutron scattering technique.[5]

The same problem that was studied in ref 5 was theoretically investigated by Honda and Kawakatsu.[9] Under a shear flow in the [111] direction of the gyroid unit cell, a nucleation and growth of the cylinder domains was observed. The gyroid arms perpendicularly oriented to the flow direction do not contribute to the formation of the cylindrical domains; i.e., they vanish during the transition. On the other hand, those that are nearly parallel to the [111] direction are elongated by the shear flow and transformed into cylinders.

Application of another type of field (e.g., electrical field) will change the nature of the transition. The difference in transition behavior was studied earlier using the sphere-to-cylinder transition as an example.[21] In the present paper we investigate the epitaxial gyroid-to-cylinder transition under an electric field using the dynamical self-consistent-field theory (SCFT). This type of transformation has not yet been studied experimentally.

2. Method

In the present work we use SCFT to study bicontinuous gyroid structure under an applied electric field. SCFT is well documented in textbooks.[22,23] SCFT is also described in detail in our recent paper on gyroid under shear flow,[9] which is closely related to the present work. Therefore, we will not repeat standard details and only mention necessary elements for the present work. We study an A−B diblock copolymer melt, with each polymer chain consisting of N_A segments of A type and N_B segments of B type. The degree of polymerization, therefore, is $N = N_A + N_B$. Our goal is to study how the morphology transforms in time under the applied electric field. For this

[†] University of Central Lancashire.
[‡] Japan Chemical Innovation Institute.
[§] Tohoku University.

10.1021/ma061875m CCC: $37.00
Published on Web 03/22/2007

purpose we use a dynamic version of SCFT, which was first proposed by Fraaije in 1993.[24] It describes time evolution of densities of various block copolymer components using a simplest possible dynamic model—diffusion type of dynamics. Polymer dynamics is a very complex phenomenon with various dynamical modes and time scales involved. The dynamical version of SCFT has no aim to describe the polymer dynamics in its full complexity, but rather to describe situations where the simple diffusion plays the major role. Examples of the characteristic time scales involved in polymer dynamics are the Rouse relaxation time, the reptation time (on a molecular level), and the time scale determined by the domain size in block copolymer system divided by the typical velocity of the block−block interface (on a mesoscopic level). If the molecular times are shorter than the mesoscale one, the use of the dynamic SCFT based on the diffusion dynamics is justified. If not, the effects of entanglements should be taken into account using extended dynamic SCFT proposed by Kawakatsu et al.[25] The diffusive dynamics is sufficient to study the phase transformations in melts or concentrated block copolymer systems. It was recently confirmed that, although being very simple, this dynamics not only reproduces the experimentally observed sequence of phases[26] but also quantitatively describes the experimentally observed phase transition kinetics in block copolymer phases.[27] An extensive discussion and estimates of the time scales described by dynamic SCFT can be found in refs 16 and 27.

In the case of applied electric field, the dynamics has the form of anisotropic diffusion type:[28]

$$\frac{\partial}{\partial t}\phi_K(\mathbf{r},t) = L_K\nabla^2\mu_K(\mathbf{r}) + \alpha\frac{\partial^2}{\partial z^2}\phi_K(\mathbf{r},t) \tag{1}$$

where ϕ_K is the local volume fraction of blocks of K-type (K = A or B), and the effect of the imposed electric field is expressed by the second term on the right-hand side (rhs) of the equation (the electric field is imposed in the z-direction). The mobility L_K (it has dimension of m^3 s/kg in SI) is taken the same for all components, i.e., $L_K = L$ for all K. The chemical potential (with the dimension of J/m^3) of blocks of K-type is defined as $\mu_K = \delta F/\delta\phi_K$, where F is the free energy of the system without an electrostatic contribution:

$$F = -MkT\ln Z + \frac{1}{2}\sum_K\sum_{K'}\int d\mathbf{r}\,\epsilon_{KK'}\phi_K(\mathbf{r},t)\,\phi_{K'}(\mathbf{r},t) - \sum_K\int d\mathbf{r}\,\phi_K(\mathbf{r},t)\,V_K(\mathbf{r},t) \tag{2}$$

where M is total number of polymer chains in the system, Z is the single chain partition function, $\epsilon_{KK'}$ is the strength of pair interaction between K- and K'-type segments, and V_K is the self-consistent potential. We consider that the system is incompressible; thus $\phi_A + \phi_B = 1$. In the case of segments of the same volume the space-averaged volume fraction of A-block is $f = \langle\phi_K(\mathbf{r},t)\rangle = N_A/N$. It is independent of time. We keep only the leading term in the electrostatic contribution to the chemical potential, expanded in a series of ϕ_K. This leads to the last term on rhs of eq 1, which makes the diffusion anisotropic in the direction of the applied electric field (z-direction in our case). The parameter, which controls this anisotropy, is[16]

$$\alpha = \frac{\epsilon_0\epsilon_1^2}{\bar{\epsilon}}E_0^2\upsilon L \tag{3}$$

where ϵ_0 is the dielectric constant of vacuum, E_0 is the amplitude of the applied electric field, and υ is the volume of a single polymer chain. The dielectric constant of a melt depends on the local volume fraction of blocks, $\phi_K(\mathbf{r},t)$. We use $\epsilon(\mathbf{r}) \approx \bar{\epsilon} + \epsilon_1(\phi_A - f)$ with $\bar{\epsilon} = \epsilon|_{\phi_A=f}$ and $\epsilon_1 = (\partial\epsilon/\partial\phi_A)|_{\phi_A=f}$.[16] Assuming $\epsilon(\mathbf{r}) = \epsilon_A\phi_A + \epsilon_B\phi_B$ (where ϵ_K is the dielectric constant of K-block), we can introduce a dimensionless parameter:[16]

$$\tilde{\alpha} = \frac{\alpha}{kTL} = \frac{\epsilon_0(\epsilon_A - \epsilon_B)^2}{\epsilon_A f + \epsilon_B(1-f)}\frac{E_0^2\upsilon}{kT} \tag{4}$$

where k is the Boltzmann constant and T is the temperature. Our treatment of the electrostatic contribution is valid provided $\epsilon_1(\phi_A - f) \ll 1$, which is the case in weak segregation regime or in intermediate segregation regime but with a weak dependence of the dielectric constant on the local composition. We refer readers to ref 16, section II, which contains a comprehensive discussion of this parameter with respect to experimental copolymer systems and electric field values.

To eliminate frustration on the block copolymer structure due to periodic boundary conditions, we apply the system size optimization (SSO) method which minimizes the free energy density of the system by optimizing the side lengths of the simulation box.[9] We use the dynamical version of SSO:[9]

$$\frac{\partial\mathscr{L}_i}{\partial t} = -\zeta_i\frac{\partial(F/V)}{\partial\mathscr{L}_i} \tag{5}$$

where $\mathscr{L}_i$ ($i = x, y, z$) are the side lengths of the simulation box, V is the system volume, and ζ_i are positive coefficients, which should be determined so that the change in the size of the simulation box does not affect the dynamics of the domains. We chose the same value of ζ_i for all sides.

For the purpose of this paper, the OCTA code,[29] which we use to perform SCFT simulations, was modified to account for the dynamics described by eq 1 with an anisotropic diffusion term.

3. Results and Discussion

3.1. Preparation of Initial G Structure. Following our previous work (Appendix D in ref 9), we start from generating a perfect gyroid (G) structure. The main idea is to start from an initial density distribution (from numerical reasons it is easier to start from SCF potential), which has G symmetry

$$\phi \propto \left[\cos 2\pi\frac{x}{D_G}\sin 2\pi\frac{y}{D_G} + \cos 2\pi\frac{y}{D_G}\sin 2\pi\frac{z}{D_G} + \cos 2\pi\frac{z}{D_G}\sin 2\pi\frac{x}{D_G}\right]^2 \tag{6}$$

where D_G is the side length of the unit cell of the G structure which can be calculated via its relation with the equilibrium spacing of the lamellar structure D_L formed by the same block copolymer of value χN. We take the same system and parameters as before: $N_A = 7$, $N_B = 13$, and $\chi N = 20$.[9] After sufficient equilibration by means of the static SCFT simulation with SSO, we obtain a perfect G system with the side length of the optimized G unit cell $D_G^0 = 17.2$ (in units of segment size that is taken to be unity), which is presented in Figure 1. To investigate the G system under an applied electric field, we choose another orientation of the G phase, which allows for investigation of the transition along the [111] direction, similar to the situation with G under shear flow studied in our previous work.[9] The three X-, Y-, and Z-axes of the new simulation box

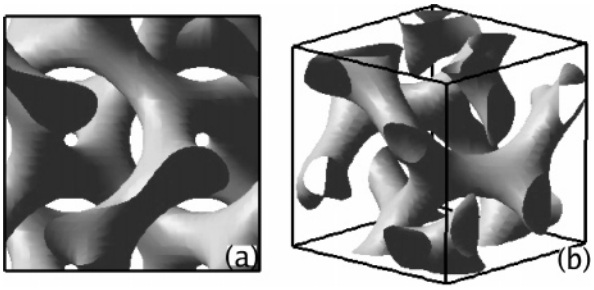

Figure 1. Two views of the perfect G structure obtained after equilibration of the structure given by eq 6. Here and in all figures below the isosurface level is $\phi_A = 0.75$.

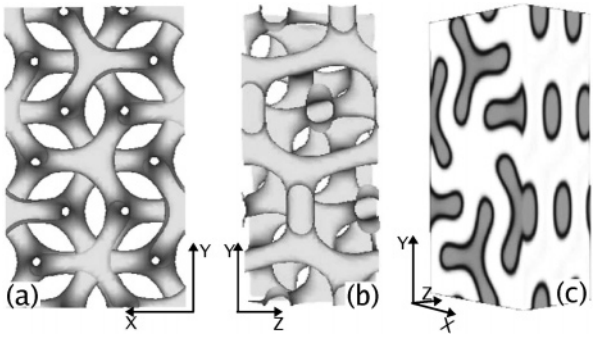

Figure 2. Different views on the perfect gyroid structure in the new simulation box with the side lengths $\sqrt{2}D_G^0$, $\sqrt{6}D_G^0$, and $(\sqrt{3}/2)D_G^0$.

are parallel to the $[1\bar{1}0]$, $[11\bar{2}]$, and [111] directions of the conventional unit cell of the G structure given by eq 6, respectively. The box sides along *X*-, *Y*-, and *Z*-axes are $\sqrt{2}D_G^0$, $\sqrt{6}D_G^0$, and $(\sqrt{3}/2)D_G^0$, respectively.[9] Such a box provides the least distortion to the gyroid structure. To simulate a bulk system, we employ periodic boundary conditions in all directions. The new box is illustrated in Figure 2. It has dimensions $36 \times 64 \times 28$ ($X \times Y \times Z$) grid units, which results in the mesh size $\Delta x = 0.68$, $\Delta x = 0.66$, $\Delta x = 0.53$ (in units of the segment size). In the following, we do not use SSO except for the very last subsection, where we discuss the effect of SSO.

3.2. Domain Dynamics during the Transition. After we have generated the initial gyroid structure, we apply an electric field along a chosen direction. The simulation parameters, which are not mentioned above, are the time step $\Delta t = 0.005$, the mobility $L_K = 1$, the mesh size along the chain $\Delta s = 0.2$, and the effective bond length is unity. Figure 3 shows results of the simulation where the electric field was applied along [111] direction, and as a result, the epitaxial transition G{211} → C{10} takes place. The *YX*-view on the structure demonstrates that arms of 3-fold G structure become thinner as time progresses while a hexagonal cylindrical structure grows from the centers of 3-folds. At a certain moment the arms are broken (Figure 3d), and the structure consists of two types of undulated cylinders, with larger and smaller degree of modulation (Figure 3e). At the end all cylinders are perfect (Figure 3f). The initiation of the cylinder phase is not seen in *XY*-view but well visible in other side views (Figure 4). In Figure 4b we see, that prior to breaking 3-fold arms, the neighboring G tripods form necks in direction on the electric field. Therefore, the intermediate structure in this transition is 5-fold connections. This process is illustrated by the five arrows in Figure 4e, which is rotated from Figure 4b a different angle. This stage is similar to the epitaxial G-to-C transition under temperature change.[20] This is very different from the G-to-C transition under shear flow, where no 5-fold connections form and 3-fold tripods are simply broken by the flow.[9] This difference lies in a fundamental difference

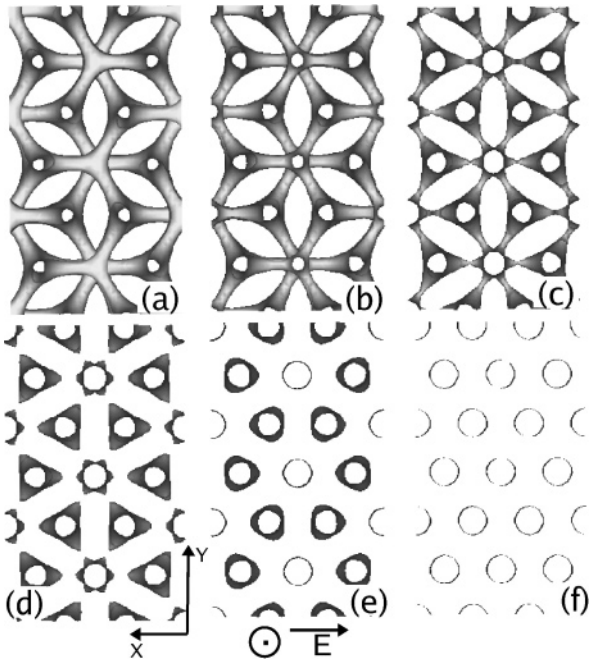

Figure 3. Kinetics of G-to-C transition under electric field applied along *Z*-axis with $\tilde{\alpha} = 0.2$. Time: t = (a) at 10, (b) 20, (c) 35, (d) 40, (e) 50, and (f) 100.

in governing time-dependent equations. In the case of the transition under shear flow it is a diffusion-convection equation with two different directions: the direction of the flow and the direction of the velocity gradient.[9] In the case of applied electric field it is anisotropic diffusion equation with only one preferred direction—direction of the electric field.[30] Additionally, there is an important difference between these two external fields. In the case of the shear, the deformation includes rotation, while the electric field case does not. This means the sheared G structure breaks in a different way from the G structure under an electric field. The difference comes from the rotational motion of the domain arms that are perpendicular to the shear direction.

Figure 4c shows that initial cylinders are undulated. The modulations seen in Figure 4c are peristaltic modulations. The modulations are suppressed by the electric field after some time (Figure 4d). Additional details of the transition are seen from the side view in Figure 5. The first three images, a−c, show how the intermediate 5-arm connections form and disappear. The next two images, d and e, show that there are two types of cylinder modulations: peristaltic and undulation (zigzag type); it can be seen from Figure 5g,h. Both types form a regular sequence in space one after another. Finally, perfect cylinders are shown in Figure 5f. A characteristic feature of this transition, Figures 3−5, is that the transition proceeds in all space with the same speed everywhere, which is different from the situation under shear flow, where coexistence of G and C phases was observed.[9]

We calculate the scattering intensities using the domain patterns obtained in the simulations. We assume that the sample consists of many gyroid crystal regions with their [111] directions (which is the *Z*-direction in our figures) being parallel to each other but with arbitrary orientation of the other crystal axes. Such an alignment is a common situation, which can be achieved, for instance, by applying a shear flow to the sample.[5] The scattering intensities were calculated by the Fourier transformation of the density fields with a proper averaging taking into account the polycrystallinity. The incoming beam

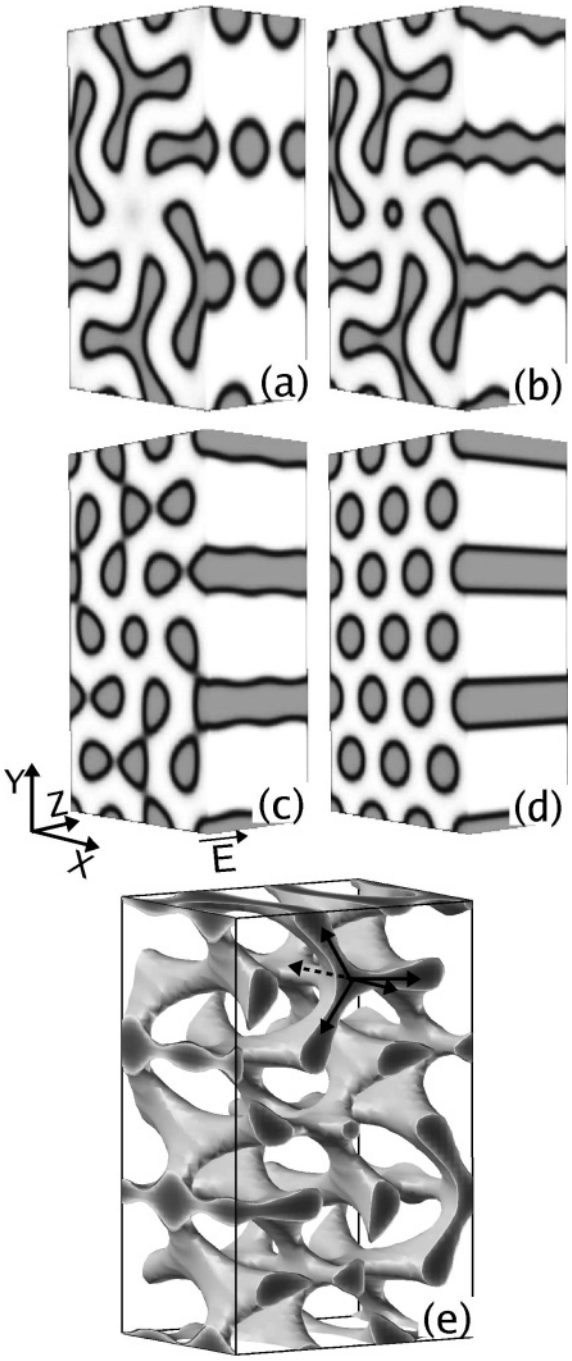

Figure 4. Different side views of the transition from Figure 3. Time: (a) at 10, (b) 20, (c) 40, and (d) 100. (e) Isovolume and isosurface at 20.

is directed perpendicularly to the [111] direction. A typical 10-spot pattern, which is characteristic of the gyroid structure,[5] is observed (Figure 6a). At the end of the G-to-C transition, characteristic 2-spots of the cylindrical phase are seen in Figure 6d. The same situation is found experimentally.[5] The most interesting result is illustrated by Figure 6b,c, which shows a disappearance of the four gyroid off-equatorial peaks and a gradual decay of the four other gyroid peaks, which are located next to the equatorial peaks. (Using the terminology of ref 5, we call those peaks equatorial which correspond to the final cylindrical structure.) This is the situation shown in the inset 6 of Figure 4 in ref 5. The experimental situation describes a relaxation of the shear-induced cylindrical structure back to the original gyroid structure after the secession of the shear flow because the gyroid structure is the equilibrium structure at that

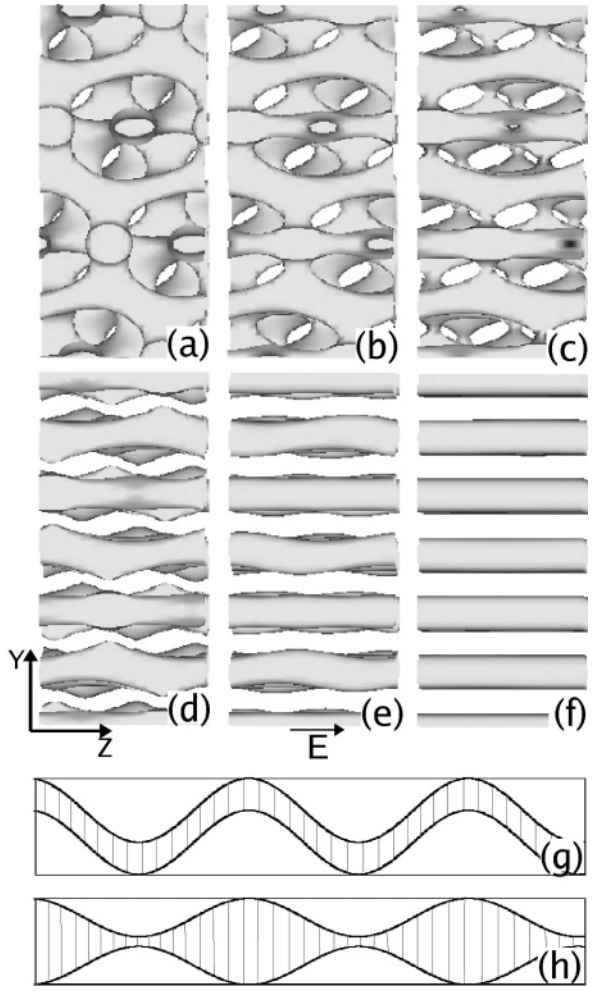

Figure 5. The same as in Figure 3 but viewed in *XZ*-plane. Time: t = (a) at 10, (b) 25, (c) 35, (d) 40, (e) 50, and (f) 100; (g) undulation type and (h) peristaltic type.[31]

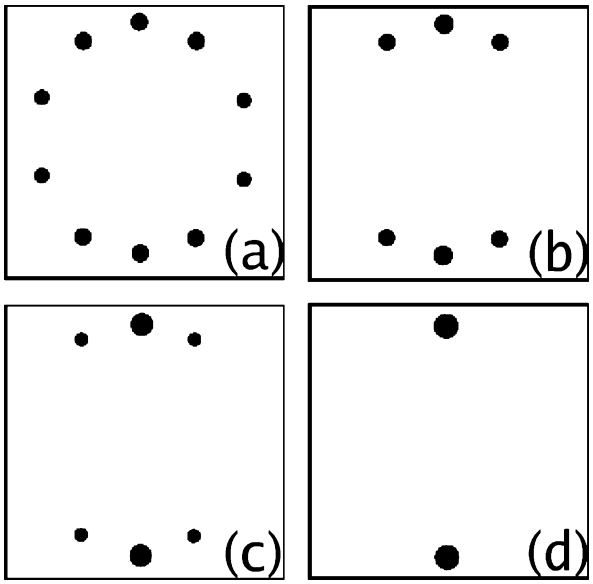

Figure 6. Intensity of scattering by the structures shown in Figures 3 and 4 in the case of the incoming beam in the $X-Y$ plane. The sample is assumed to be a polycrystal with all possible domain orientations around the Z ([111]) axis. The area of each spot is proportional to the intensity. Time: t = (a) 0, (b) 10, (c) 20, and (d) 100.

temperature. As we see the same transition state under an applied electric field (Figure 6b), the effect of the electric field is supposingly similar to a change in the temperature. We elaborate

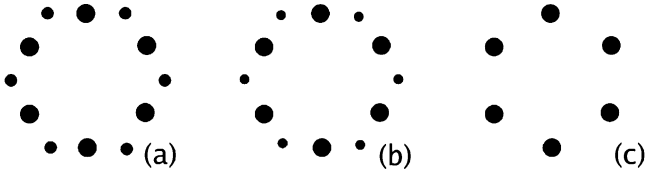

Figure 7. Intensity of scattering by the structures shown in Figures 3 and 4 in the case of the incoming beam is in the [111] direction. The sample is a monocrystal as shown in Figure 3. Time: t = (a) 0, (b) 20, and (c) 100.

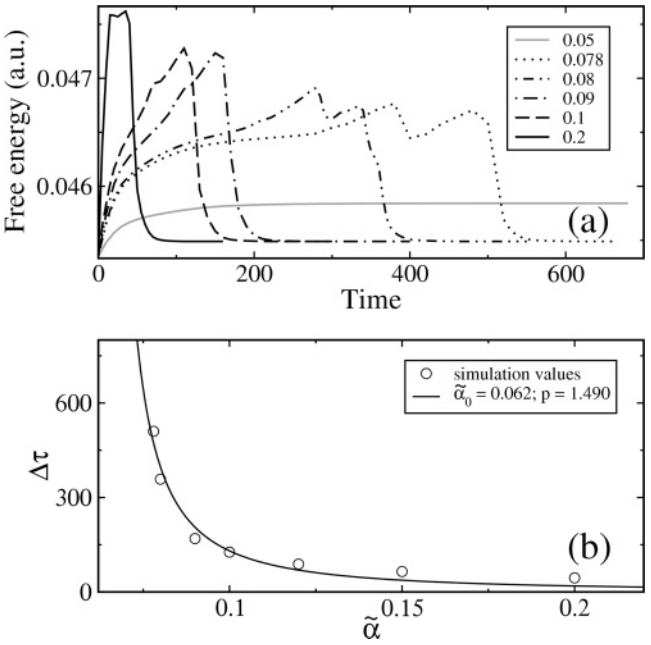

Figure 8. (a) Free energy in arbitrary units (au) as a function of time for different values of applied field $\tilde{\alpha}$. (b) Total time of the transition as a function of electric field; solid line is fitting by function $\Delta\tau = (\tilde{\alpha} - \tilde{\alpha}_0)^{-p}$.

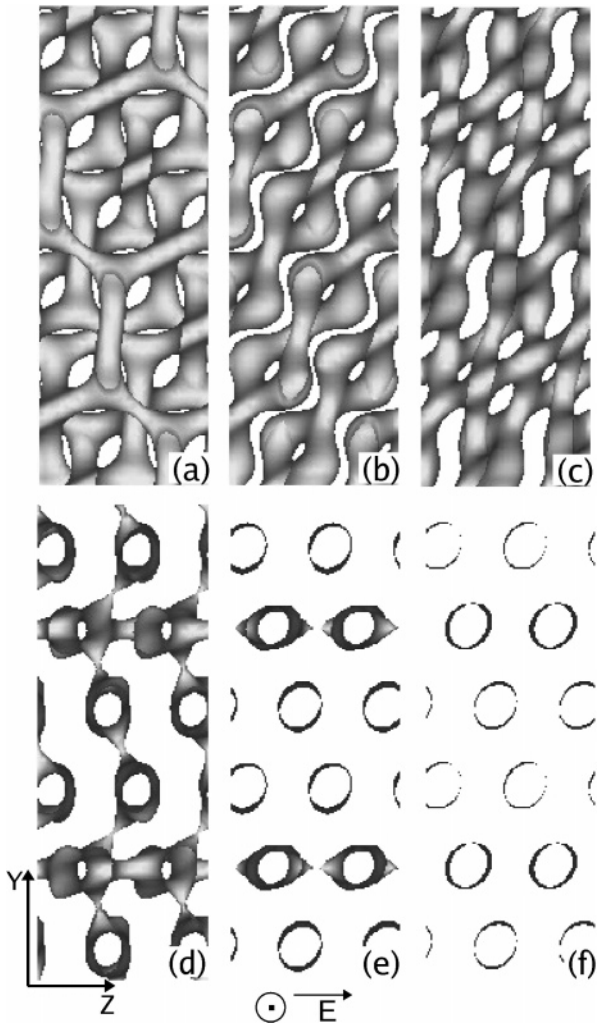

Figure 9. Kinetics of G-to-C transition under electric field applied along X-axis with $\tilde{\alpha} = 0.2$. Time: t = (a) at 60, (b) 130, (c) 180, (d) 365, (e) 430, and (f) 480.

on that issue in the following subsection. Moreover, nonsimultaneous evolution of the above-mentioned eight peaks (peaks C and D in the notation of ref 5) was found surprising and attributed to a possible "dependence of the growth rate on the rotational position of the morphology with respect to the shear geometry".[5] We can confirm that this is not the case, and the 6-spot patterns from Figure 6b,c correspond to the development of the intermediate structures in the G-to-C transition, which includes a formation of the 5-fold connections and various undulations of the network arms.

Figure 7 shows scattering in a different direction, namely along the Z ([111]) direction. In this case the sample should be a monocrystal to observe separate peaks and not circles. The initial gyroid structure is seen as superposition of two hexagons in reciprocal space, rotated by $\pi/3$ with respect to each other and having slightly different wave vectors (Figure 7a). In the course of time, one hexagon dies out (Figure 7b), and only one remains, which corresponds to the hexagonally packed cylinders (Figure 7c). Scattering in this direction was not done experimentally but can be performed, if a sufficiently large gyroid monocrystal can be obtained (possibly by a temperature change from the initial state of hexagonally packed perpendicular cylinders in a thin film).

3.3. Lifetime of the Initial G Phase. The simulations have been carried out for various values of the electric field. Figure 8a shows the free energy as a function of time for several values of the applied field. Following our previous work,[16] we have chosen to illustrate the transition by the free energy without the electrostatic contribution. This partial free energy provides a measure of the change in the strength of the microphase separation. It reflects the changes in shapes and connectivity of domains, just like the case in our previous work on cylindrical domains under external electric field.[16] The electric field is applied at the time $t = 0$. It serves as a disturbance to the system, which manifests itself by a sharp increase in the free energy shortly after $t = 0$. At this initial stage the system reduces the strength of its phase separation to some extent (i.e., the interfaces become more diffuse and the contrast between the two domains becomes smaller), as the application of an electric field is similar to a shift in the temperature.[32] If the electric field is weak (see, for instance, the line for $\tilde{\alpha} = 0.05$), the free energy reaches a plateau and the system remains in the gyroid phase but with a slightly increased free energy. We call this state an "excited gyroid". If the field is above a certain threshold value (the lines with $\tilde{\alpha} = 0.078$ and above), such an "excited gyroid" has a finite lifetime. When this time elapses, the free energy drops to another plateau, which corresponds to a cylindrical phase. For all values of the electric field the height of the second plateau is the same, which reflects the fact that the final cylindrical phase is the same for all fields as long as the transition occurs. The details of this transition have been discussed in Figures 9−11. The time duration of the transition, which is defined as the time span of the free energy drop (from the start of the drop until the second plateau in Figure 8), is approximately the same

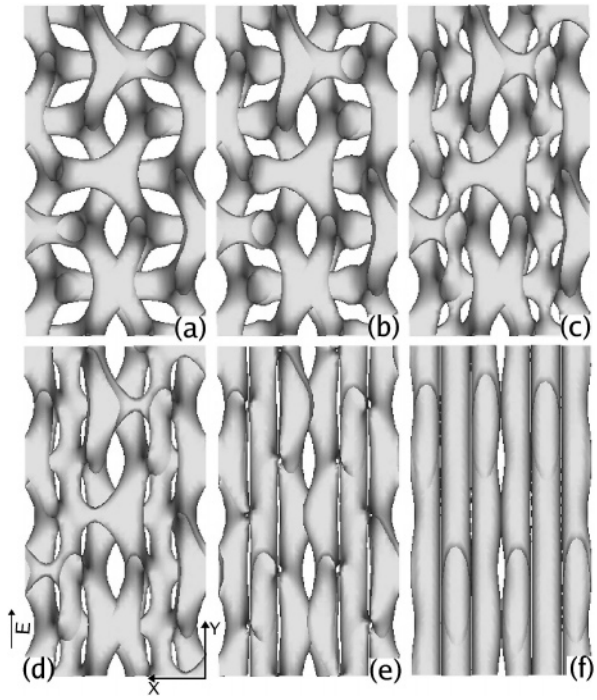

Figure 10. Kinetics of G-to-C transition under electric field applied along the *Y*-axis with $\tilde{\alpha} = 0.2$. Time: (a) at 10, (b) 20, (c) 30, (d) 40, (e) 60, and (f) 100.

for all values of the electric field, while the lifetime of the "excited gyroid" in the applied electric field until its transformation to cylinders is distinctly different for different values of the electric field.

The situation of the "excited" structure is similar to the one observed in the reorientation of cylinders in an electric field (see ref 16, Figure 7). We evaluate the lifetime $\Delta\tau$ of an "excited" structure from the graphs in Figure 8a as the time span from $t = 0$ (when the electric field was applied) until the moment of the half-height of the drop in the free energy. The result is shown in Figure 8b. The values of the lifetime diverges as the strength of the electric field decreases. This suggests that we can discuss this transition in terms of critical phenomena and fit the data using the argument of critical exponents. The result is shown in Figure 8b. The threshold value of the electric field is found to be $\tilde{\alpha}_0 = 0.062$ with critical exponent $p = 1.49$. Intuitively, this can be explained by the following arguments. In the Landau theory of the phase transition of the second order, the correlation length behaves as $(T - T_c)^{-1/2}$ in the vicinity of the critical temperature T_c. On the other hand, the Lifshitz−Slyozov theory on the time evolution of the characteristic length of a conserved order parameter follows $\tau^{1/3}$.[32] Combining these two relations gives $\tau = (T - T_c)^{-3/2}$. This can be understood as follows. The electrostatic contribution to the free energy renormalizes the coefficient of the ϕ^2 term in the free energy.[32] This renormalization leads to a shift of the critical temperature. Such a change causes a critical phenomenon.

3.4. Electric Field in Other Directions. We have also carried out two simulations where the applied electric field is directed along the other two directions, i.e., along *X* ($[1\bar{1}0]$) or *Y* ($[11\bar{2}]$) directions. The results are shown in Figures 9−11. In all cases we obtain the cylindrical phase at the end, but kinetics of the transition is different from what we discussed above. The most significant difference is seen in the transition illustrated in Figure 9. In the initial stage G structure starts to change the strength of its microphase separation (the structure is becoming thinner due to partial melting) without observable change in the topology of the domain structure (compare Figures 2b and 9a). This is due to the effective change in the temperature difference $(T - T_c)$, as described in the previous subsection. In the next stage the system splits into a set of disconnected wavy laces (Figure 9b), which become again interconnected after a short while (Figure 9c). In the later stage a transition to cylinders aligned along the *X*-axis occurs. The transition does not happen homogeneously in the whole system (Figure 9d,e), contrary to the situation when the field was along the *Z*-axis (Figure 3). The final hexagonal structure is a bit distorted (Figure 9f), which can be attributed to the effect of the small *Z*-side of the simulation box. The situation in the case of the field applied along the *Y*-axis is different, as is shown in Figures 10 and 11:

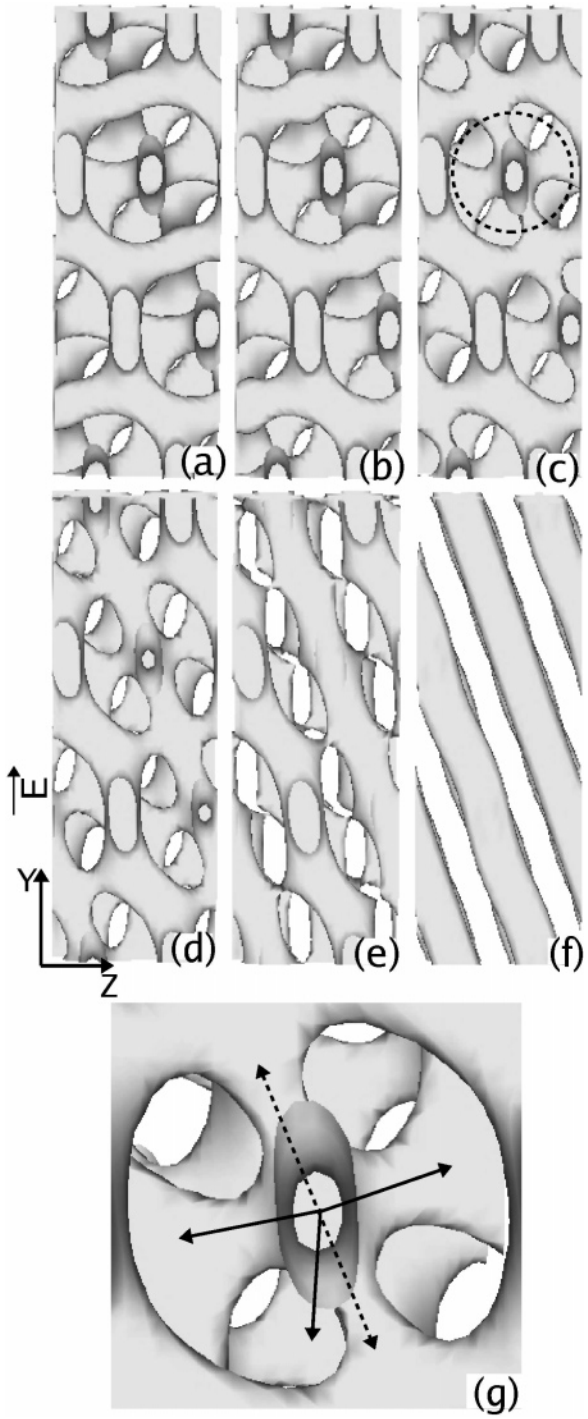

Figure 11. The same as in Figure 10 but viewed in the *YZ*-plane. Time: $t =$ (a) at 10, (b) 20, (c) 30, (d) 40, (e) 60, and (f) 100. (g) Close-up 5-fold connection from (c).

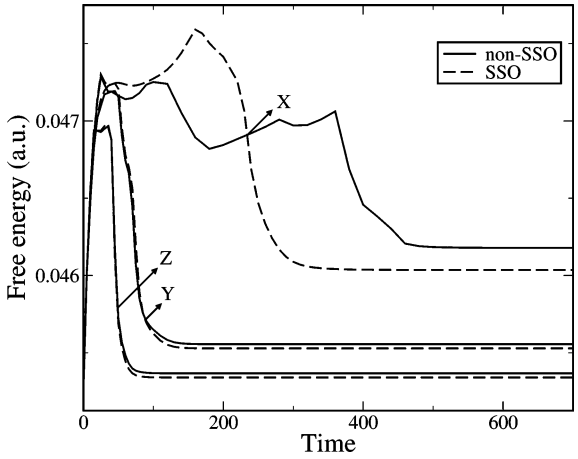

Figure 12. Free energy in arbitrary units (au) as a function of time for different directions *X*, *Y*, *Z* with $\tilde{\alpha} = 0.2$.

the transition proceeds homogeneously in the whole simulation box, similar to the case illustrated in Figure 5. The system also forms an intermediate structure with nodes having more connections compared to 3-fold connections of gyroid (Figures 10c and 11c). A typical 5-fold connection is shown in Figure 11g. Formation of an intermediate with more than 3-fold connections is similar to the situation of the applied electric field along *Z*-axis, but the orientation of the new structure is different. Simply due to the geometry of the G phase, new connections are forming not parallel to the electric field but in a tilted direction (Figure 11a−e). As a result, newly formed cylinders are tilted as well (Figure 11f). Under the periodic boundary condition, a cylindrical domain that crosses the boundary and tilted to the side of the simulation box cannot reorient to the parallel direction of the simulation box unless it breaks. Therefore, the structure is trapped in this state, similar to the situation discussed for lamellar case in ref 28. The free energy as a function of time is shown in Figure 12 for different directions of the applied electric field (solid lines). It demonstrates that the speed of the transition is the fastest if the electric field is applied along *Z* ([111]) direction and is the slowest if it is along *X* ([$1\bar{1}0$]) direction. Therefore, the instability modes shown in Figure 4 are the fastest growing modes and will be the ones realized in experiments, where the initial gyroid sample is a polycrystal with different orientations of domains.

3.5. Effects of SSO. The results we showed above are for calculations without SSO. To elaborate on the issue of possible structural frustration due to a small simulation box, we carry out calculations with SSO as well. We use the value of parameter ζ_i in eq 5 equal to 1. Figure 12 shows free energy as a function of time for both types of simulations: with SSO and without SSO. In the cases of an electric field applied in *Y*- or *Z*-directions, the results are not much different between simulations with SSO and without SSO. However, with SSO involved, we obtain the cylindrical structure with a lower free energy. Therefore, the final structure is more perfect. The situation is quite different in the case of the field in the *X*-direction. A simulation with SSO shows a drastically different kinetics. The transition occurs almost twice as early as in the case without SSO (Figures 9e and 13e; see also Figure 12, dashed "X" curve). Contrary to the situation described in Figure 9, the transition calculated with SSO (Figure 13) proceeds homogeneously in the whole simulation box. There is no intermediate state with disconnected waves like one in Figure 9b, which is followed by the interconnected structure in Figure 9c. Instead, when a wavy disconnected pattern is formed (Figure 13d), it is directly

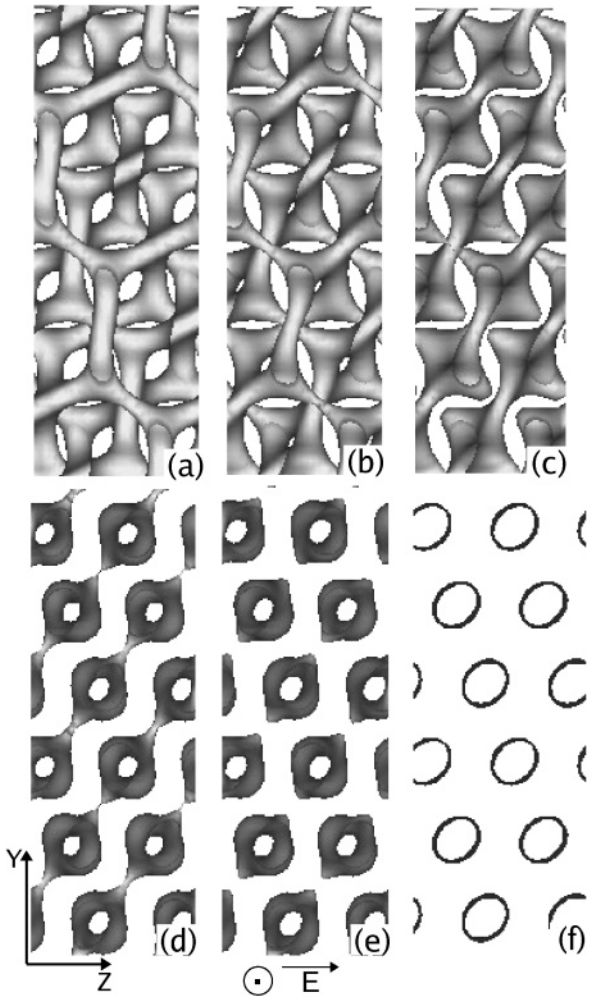

Figure 13. Kinetics of G-to-C transition under electric field applied along *X*-axis, $\tilde{\alpha} = 0.2$, with SSO involved. Time: $t =$ (a) at 60, (b) 130, (c) 165, (d) 225, (e) 230, and (f) 300.

followed by the formation of cylinders. The final cylinders (Figure 13f) are still slightly distorted in the *YZ*-plane even with SSO. Therefore, we can conclude that in the absence of structural defects the transition will be always homogeneous in space.

4. Conclusion

By using the real-space dynamical SCF method, we have calculated the epitaxial transition gyroid → cylinder under an electric field. A threshold value of the applied electric field is required to induce the transition. The time of the transition diverges at this value with the critical exponent 3/2, which can be understood using mean-field theory of the second-order phase transition. We show details of the kinetics of the transition, which includes intermediate structures with increased connectivity compared to the gyroid phase. The transition under the electric field proceeds homogeneously in space, contrary to the similar transition under a shear flow. We have found that the fastest growing instability modes are realized, if the field is along [111] of gyroid conventional unit cell. We also have used SSO method, which helps us to conclude that structural defects serve as nuclei for the transition, and in their absence the transition will be homogeneous in space.

Acknowledgment. This work is partially supported by the national project on nanostructured polymeric materials, which has been entrusted to the Japan Chemical Innovation Institute

by the New Energy and Industrial Technology Development Organization (NEDO) under METI's Program for the Scientific Technology Development for Industries that Creates New Industries. It is also supported by a grant-in-aid for the priority area "Non-equilibrium Soft Matter Physics" from the Ministry of Education, Culture, Sports, Science, and Technology, Japan. All simulations were performed on a SGI Altix 3700 supercomputer at UCLan High Performance Computing Facilities (UK).

References and Notes

(1) Bates, F. S.; Fredrickson, G. H. *Annu. Rev. Phys. Chem.* **1990**, *41*, 5252.
(2) Hamley, I. W. *The Physics of Block Copolymers*; Oxford University Press: Oxford, 1998.
(3) Schulz, M. F.; Bates, F. S.; Almdal, K.; Mortensen, K. *Phys. Rev. Lett.* **1994**, *73*, 86.
(4) Förster, S.; Khandpur, A. K.; Zhao, J.; Bates, F. S.; Hampley, I. W.; Ryan, A. J.; Bras, W. *Macromolecules* **1994**, *27*, 6922.
(5) Eskimergen, R.; Mortensen, K.; Vigild, M. E. *Macromolecules* **2005**, *38*, 1286.
(6) Wang, C. Y.; Lodge, T. P. *Macromolecules* **2002**, *35*, 6997.
(7) Zvelindovsky, A. V.; Sevink, G. J. A.; van Vlimeren, B. A. C.; Maurits, N. M.; Fraaije, J. G. E. M. *Phys. Rev. E* **1998**, *57*, R4879.
(8) Kodama, H.; Doi, M. *Macromolecules* **1996**, *29*, 2652.
(9) Honda, T.; Kawakatsu, T. *Macromolecules* **2006**, *39*, 2340.
(10) Gurovich, E. *Macromolecules* **1994**, *27*, 7339.
(11) Onuki, A.; Fukuda, J. *Macromolecules* **1995**, *28*, 8788.
(12) Pereira, G. G.; Williams, D. R. M. *Macromolecules* **1999**, *32*, 8115.
(13) Ashok, B.; Muthukumar, M.; Russell, T. P. *J. Chem. Phys.* **2003**, *115*, 1559.
(14) Tsori, Y.; Tournilhac, F.; Andelman, D.; Leibler, L. *Phys. Rev. Lett.* **2003**, *90*, 145504.
(15) Xu, T.; Zvelindovsky, A. V.; Sevink, G. J. A.; Gang, O.; Ocko, B.; Zhu, Y.; Gido, S. P.; Russell, T. P. *Macromolecules* **2004**, *37*, 6980.
(16) Lyakhova, K. S.; Zvelindovsky, A. V.; Sevink, G. J. A. *Macromolecules* **2006**, *39*, 3024.
(17) Holmes, M. C.; Leaver, S. M. Intermediate Phases. In *Bicontinuous Liquid Crystals*; Lynch, M. L., Spicer, P. T., Eds.; Taylor & Francis: New York, 2005.
(18) Hashimoto, T.; Tsutsumi, K.; Funaki, Y. *Langmuir* **1997**, *13*, 6869−6872.
(19) Alexander, C. E.; Augustine, M. U.; DeRege, P.; Chen, C. X.; Swager, T. M.; Hadjichristidis, N.; Xenidou, M.; Fetters, L. J.; Joannopoulos, J. D.; Fink, Y.; Thomas, E. L. *Adv. Mater.* **2001**, *13*, 421−425.
(20) Matsen, M. W. *Phys. Rev. Lett.* **1998**, *80*, 4470.
(21) Pinna, M.; Zvelindovsky, A. V.; Todd, S.; Goldbeck-Wood, G. *J. Chem. Phys.* **2006**, *125*, 154905.
(22) Kawakatsu, T. *Statistical Physics of Polymers: An Introduction*; Springer: Berlin, 2004.
(23) Matsen, M. W. Self-Consistent Field Theory and Its Applications. In *Soft Matter*; Gompper, G., Schick, M., Eds.; Wiley: Weinheim, 2006; Vol. 1.
(24) Fraaije, J. G. E. M. *J. Chem. Phys.* **1993**, *99*, 9202.
(25) Shima, T.; Kuni, H.; Okabe, Y.; Doi, M.; Yuan, X.-F.; Kawakatsu, T. *Macromolecules* **2003**, *36*, 9199.
(26) Knoll, A.; Horvat, A.; Lyakhova, K. S.; Krausch, G.; Sevink, G. J. A.; Zvelindovsky, A. V.; Magerle, R. *Phys. Rev. Lett.* **2002**, *89*, 035501.
(27) Knoll, A.; Lyakhova, K. S.; Horvat, A.; Krausch, G.; Sevink, G. J. A.; Zvelindovsky, A. V.; Magerle, R. *Nat. Mater.* **2004**, *3*, 886.
(28) Zvelindovsky, A. V.; Sevink, G. J. A. *Phys. Rev. Lett.* **2003**, *90*, 049601.
(29) Honda, T.; Kodama, H.; Roan, J.-R.; Morita, H.; Urashita, S.; Hasegawa, R.; Yokomizo, K.; Kawakatsu, T.; Doi, M. *SUSHI Users Manual*; OCTA: Nagoya, Japan, 2004 (http://octa.jp).
(30) Zvelindovsky, A. V.; Sevink, G. J. A. *J. Chem. Phys.* **2005**, *123*, 074903.
(31) van der Linden, E.; Menger, F. M. *Langmuir* **1993**, *9*, 690.
(32) Onuki, A. *Phase Transition Dynamics*; Cambridge University Press: Cambridge, 2002.

MA061875M